

Electron-Deficient Compounds

A Soluble Ladder-Conjugated Star-Shaped Oligomer Composed of Four Perylene Diimide Branches and a Fluorene Core: Synthesis and Properties

Youdi Zhang, Lingcheng Chen,* Kaichen Zhang, Helin Wang, and Yi Xiao*[a]

Abstract: A new ladder-conjugated star-shaped oligomer electron-transporting material **TetraPDI-PF**, with four perylene diimide (PDI) branches and a fluorene core, was efficiently synthesized. The oligomer is highly soluble in dichlorobenzene with a solubility of 155 mg mL⁻¹, which is higher than those of PDI (35 mg mL⁻¹) and **PDI-Phen** (70 mg mL⁻¹). Demonstrated by thermogravimetric analysis (TGA), the oligomer exhibits excellent thermal stability with the decomposition temperature (T_d) of 291.2 °C, which is 65 °C higher than that of PDI. Cyclic voltammetry (CV) and differential pulse voltammetry (DPV) were employed to investigate the electrochemical properties. Although the CV curves of **TetraPDI-PF** are successively scanned for 15 cycles, they still

remain invariable reduction potentials. The oligomer also shows outstanding photostability, even better than PDI, which maintains 99% fluorescence intensity after irradiation for 10 min using maximum laser intensity. In the steady-state space-charge-limited current (SCLC) devices, **TetraPDI-PF** exhibits higher intrinsic electron mobility of $2.22 \times 10^{-5} \text{ cm}^2 \text{ V}^{-1} \text{ s}^{-1}$, three orders of magnitude over that of PDI ($3.52 \times 10^{-8} \text{ cm}^2 \text{ V}^{-1} \text{ s}^{-1}$). The bulk heterojunction (BHJ) organic solar cells (OSCs) using **TetraPDI-PF** as non-fullerene acceptors and P3HT as donors give optimum power conversion efficiency (PCE) of 0.64%, which is 64 times that of the PDI:P3HT BHJ cells.

Introduction

The design of new N-type (electron-transporting) organic semiconductors is an essential work for the fields related to organic electronics, because the development of N-type materials lags far behind P-type (hole-transporting) materials.^[1] Although there are plenty of excellent P-type organic semiconductors,^[2] the efficient and stable N-type counterparts are still rare,^[3] though both of them are indispensable for most electronic devices.

A current trend is emerging to develop new soluble N-type ladder-conjugated molecules.^[4] Conventionally, several classes of N-type ladder-conjugated polymers, such as **BBL** (Figure 1),^[5] are good organic semiconductors with satisfactory electron mobility and stability, because of their large, rigid, and planar frameworks with highly extended conjugation systems. However, such ladder frameworks also result in extremely poor solubility, which hampers the applications in solution-processed organic electron devices. To address this problem, large and flexible alkyl side chains have been introduced to enhance the solubility. For example, very recently, Jenekhe et al. have

reported soluble BFI-T2 that show high electron mobility up to $0.12 \text{ cm}^2 \text{ V}^{-1} \text{ s}^{-1}$ in organic field-effect transistors and an efficiency of 1.80% in BHJ Cells (Figure 1).^[6] Another excellent example is from the group of Müllen who synthesized processable perylene diimide dyes of 4 nm in length.^[7]

From another perspective, quite a few star-shaped P-type molecules exhibit good solubility, because, to some extents, their flexible and non-planar branches inhibit the aggregation effect caused by the aromatic cores.^[8] In some cases, the coordination of the branches and the core can even produce discotic or columnar liquid crystalline structures as the preferred charge-transporting pathways.^[9] However, there are rare reports on the design of star-shaped N-type materials.^[8a,10] Even so, we still believe that the strategy to improve solubility by the construction of star-shaped molecules should also be applicable for addressing the problem of ladder-conjugated N-type conjugated materials.

For several years, our group has been engaged in the development of soluble N-type ladder-conjugated molecules based on perylene diimide (PDI) derivatives that have outstanding electron mobility, strong light absorption, and high photostability and thermal stability (Figure 1). In 2011, we synthesized **LCPT**, the first PDI-based ladder conjugated polymer through photocyclization within the corresponding PDI-thienothiophene single-stranded conjugated polymer.^[11] In addition, in 2012, we reported **Tr-PBI**, a star-shaped oligomer containing three PDI branches and using truxene as the core.^[12] Furthermore, in 2013, we developed **TriPBI**, another three-PBI star-shaped molecule with hexaazatriphenylene as the core.^[13]

[a] Y. Zhang, Dr. L. Chen, K. Zhang, H. Wang, Prof. Y. Xiao
State Key Laboratory of Fine Chemicals
Dalian University of Technology, Dalian 116024 (P.R. China)
Fax: (+86) 411-84986252
E-mail: lcchen@dlut.edu.cn
xiaoyi@dlut.edu.cn

Supporting information for this article is available on the WWW under <http://dx.doi.org/10.1002/chem.201402100>.

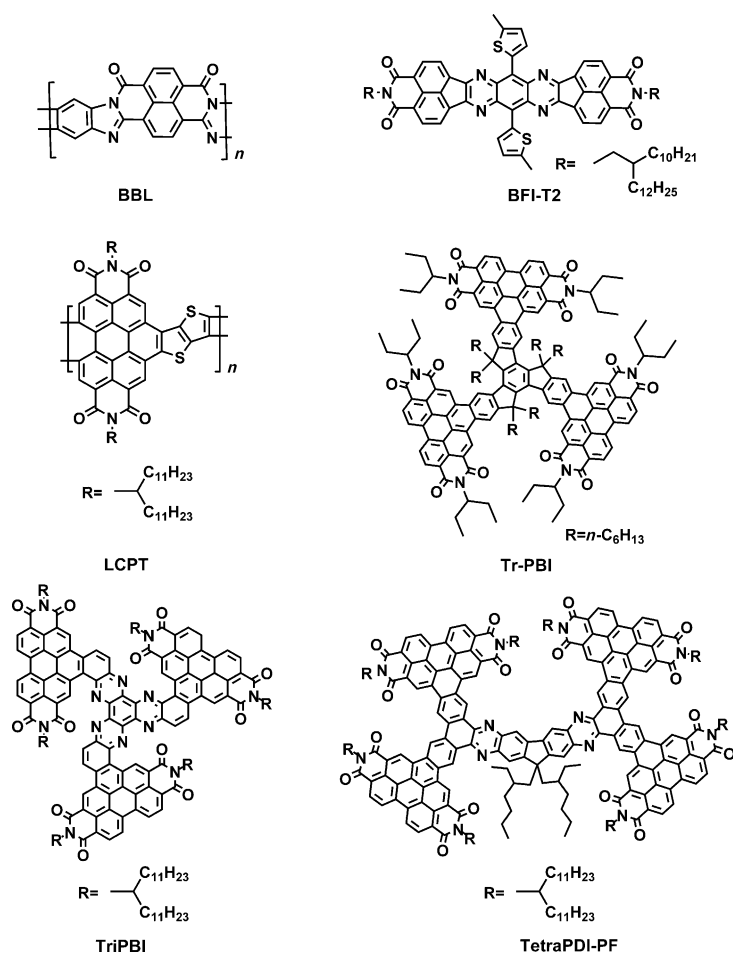


Figure 1. The structures of BBL, BFI-T2, LCPT, Tr-PBI, TriPBI, and TetraPDI-PF.

These soluble ladder-type conjugated molecules demonstrated intriguing optoelectronic properties.

In this contribution, we have developed a new star-shaped ladder-conjugated molecule **TetraPDI-PF** with four PDI branches and a fluorene core (Figure 1). In our strategy, the center core 2,3,6,7-tetraamino-9,9-bis(2-ethylhexyl)fluorene (**TABEF**) can efficiently inhibit the aggregation and enhance the solubility.^[14] In addition, we have designed a bulky branch containing two PDI branches, as a universal building block framework, in which the larger branch will extend conjugation for better electron delocalization and higher charge mobility. The molecule **TetraPDI-PF** is found to have high solubility of 155 mg mL⁻¹ in dichlorobenzene and excellent thermal, electrochemical, and photostabilities. Meanwhile, we have investigated the electron mobility and the photovoltaic performance with **TetraPDI-PF** as electron acceptors and P3HT as electron donors.

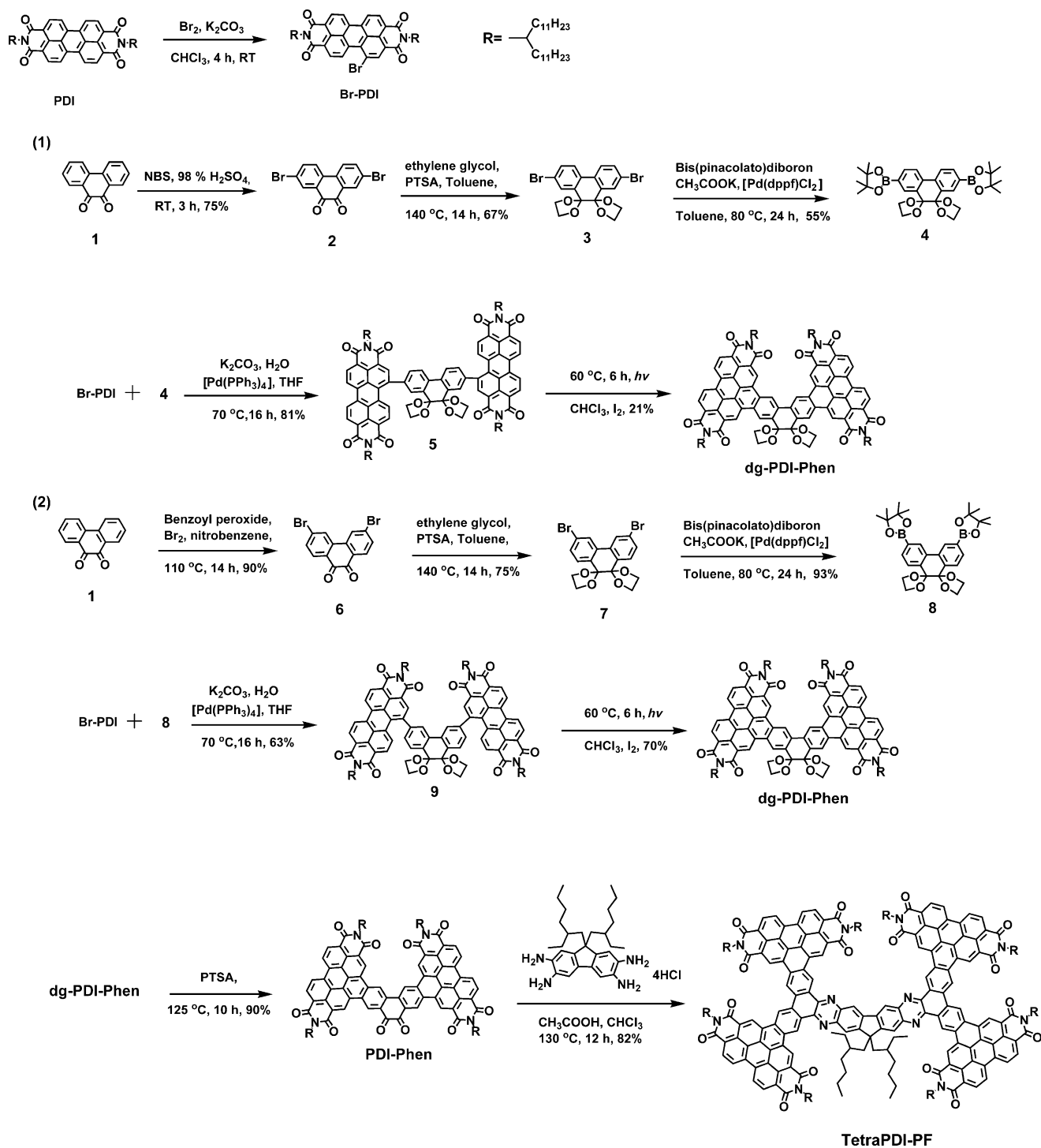
Results and Discussion

Scheme 1 shows two strategies to synthesize the target compound **TetraPDI-PF**. Firstly, with phenanthrenequinone as the starting material, 2,7-dibromo-phenanthrenequinone and 3,6-dibromo-phenanthrenequinone are efficiently synthesized in

high yields of 75 and 90%, respectively. Secondly, the coupling products, synthesized by Suzuki coupling reaction between Br-PDI and phenanthrenequinone boric acid ester with a 2,7-position or 3,6-position, using [Pd⁰(PPh₃)₄] as the catalyst in a mixture of toluene and an aqueous solution of K₂CO₃ (2 M), are transformed into the uniform intermediate **dg-PDI-Phen** containing the protection of diethylene glycol by photoinduced cyclization in the presence of a catalytic amount of iodine. As a result, **dg-PDI-Phen** is obtained with a higher yield of 70% by the 3,6-position coupling product, whereas a yield of 21% was achieved by the one in the 2,7-position. Thirdly, **PDI-Phen**, an enlarging conjugated pivotal intermediate, is synthesized efficiently by deprotecting in anhydrous *p*-toluene sulfonic acid (PTSA). **PDI-Phen** containing two adjacent carbonyl groups could fuse with any kind of aromatic systems that have two adjacent amino groups. Therefore, **PDI-Phen**, as a universal building block, is a valuable intermediate that develops and explores more suitable organic N-type materials applied in organic electronics. Finally, a new ladder-conjugated star-shaped molecule **TetraPDI-PF** containing a **TABEF** core fused with two **PDI-Phen** arms was synthesized efficiently in the mixing solution of glacial acetic acid and chloroform (CH₃COOH/CHCl₃, v/v 1:1).

It should be noted that solubility plays an important role in solution-processed organic electronic devices. We measured their solubility in common organic solution, and found that the solubility of PDI is 65, 50, and 35 mg mL⁻¹ in chloroform, chlorobenzene, and dichlorobenzene solution, respectively. The solubility of **PDI-Phen** is 100, 85, and 70 mg mL⁻¹ in chloroform, chlorobenzene, and dichlorobenzene solution, respectively. Compared with PDI and **PDI-Phen**, **TetraPDI-PF** has excellent solubility of 205, 170, and 155 mg mL⁻¹ in chloroform, chlorobenzene, and dichlorobenzene solution, respectively. These results reveal that the improvement of solubility is mainly due to the congestion and the rigidity of the conjugated framework in which the steric hindrance results in a non-coplanar structure. As demonstrated by quantum-chemical calculations using density functional theory (DFT) (Figure 2 and the Supporting Information, Figure S1), there exists a maximum molecular planar distortion of 13.31° between center core and PDI branch. In addition, two 2-ethylhexyl chains, introduced to the 9, 9'-position of fluorene core, can form the definite steric hindrance, which efficiently inhibits the aggregation and further enhances the solubility.

It is crucial to obtain the thermal stability of the star-shaped molecule as they provide important reference information for thermal annealing temperature in organic electronic devices. The thermal stability is evaluated by thermogravimetric analysis (TGA) in nitrogen with a heating rate of 10 °C min⁻¹. As shown in Figure 3, PDI, **PDI-Phen**, and **TetraPDI-PF** possess thermal stability with the decomposition temperature (*T_d*) of 225.8, 251.8, and 291.2 °C, respectively. Although the number



Scheme 1. Synthesis of the target compound **TetraPDI-PF** and two synthetic pathways of **dg-PDI-Phen**.

of flexible chains within **TetraPDI-PF** is increased, in comparison with PDI and **PDI-Phen**, it does not accelerate the decomposition, which means the rigid conjugated skeleton of this large star-shaped oligomer plays a major role in the process of the thermal decomposition. As a result, the T_d of **TetraPDI-PF** is 65 °C higher than that of PDI. The results reveal that the star-shaped ladder-conjugated molecule has an excellent thermal stability, which should be ascribed to the extension of large rigid conjugated system.

The absorption and emission spectra of PDI, **PDI-Phen**, and **TetraPDI-PF** in dichloromethane ($1 \times 10^{-5} \text{ mol L}^{-1}$) and in films are shown in Figure 4a–4d, and the relative data are shown in Table 1. As shown in Figure 4a, they exhibit sharp peaks in almost different multiple bands. PDI shows a narrow absorption spectra from 450 to 550 nm and a maximum absorption peak at 525 nm ($\epsilon = 8320 \text{ m}^{-1} \text{ cm}^{-1}$) and the maximum absorption peak of **PDI-Phen** is at 435 nm ($\epsilon = 7000 \text{ m}^{-1} \text{ cm}^{-1}$). Compared with the two ones, **TetraPDI-PF** shows stronger and

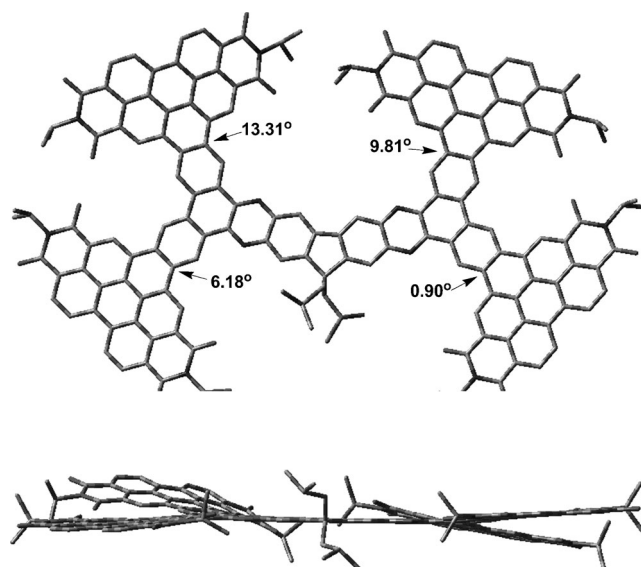


Figure 2. Ground-state geometries of **TetraPDI-PF** calculated from density functional theory.

broader absorption spectra. The absorption spectra cover a broad wavelength range from 300 to 550 nm. The shorter wavelength absorption bands at 325 nm is originated from the $\pi-\pi^*$ transition and the maximum absorption peak is at 481 nm ($\epsilon = 25700 \text{ M}^{-1} \text{ cm}^{-1}$). These results reveal that the enlarged conjugated system benefits the efficient absorption of the solar spectrum. And the optical energy band gaps (E_g^{opt}) of PDI, **PDI-Phen** and **TetraPDI-PF**, deriving from the absorption onset, are 2.3, 2.24, and 2.26 eV, respectively. In the films (Figure 4b), they show obvious redshifts relative to those in solution and exhibit significant broader absorption over 580 nm with the maximum absorption peaks of 497, 492, and 488 nm for PDI, **PDI-Phen**, and **TetraPDI-PF**, respectively. Compared with the other twos, **TetraPDI-PF** shows blueshifts of the maximum peak and absorption edge in the film, which indicate the large rigid structure could inhibit intermolecular aggregation.

The emission spectra of PDI have a peak at 534 nm in dichloromethane (Figure 4c). With the increase of the conjugated framework, the large redshifts of 36 and 50 nm for the emission maximum of **PDI-Phen** and **TetraPDI-PF** are observed. And as shown in Figure 4d, PDI displays a strong fluorescence emission in thin films. However, the fluorescence intensity of **PDI-Phen** is relatively weakened and **TetraPDI-PF** shows strong fluorescence quenching. The weak fluorescence emission of **TetraPDI-PF** will benefit to the charge separation in the organic solar cells (OSCs).

The cyclic voltammetry (CV) and differential pulse voltammetry (DPV) are employed to investigate the electrochemical properties and determine the highest occupied molecular orbital (HOMO) and the lowest unoccupied molecular orbital (LUMO) energy levels of PDI, **PDI-Phen**, and **TetraPDI-PF** (Figure 4e–g and the Supporting Information, Figure S2), and the relative data are shown in Table 1. PDI shows two reversible reduction waves, whereas **PDI-Phen** and **TetraPDI-PF** show three and four reversible reduction waves, respectively, indicating their ability to accept at least three electrons. More impor-

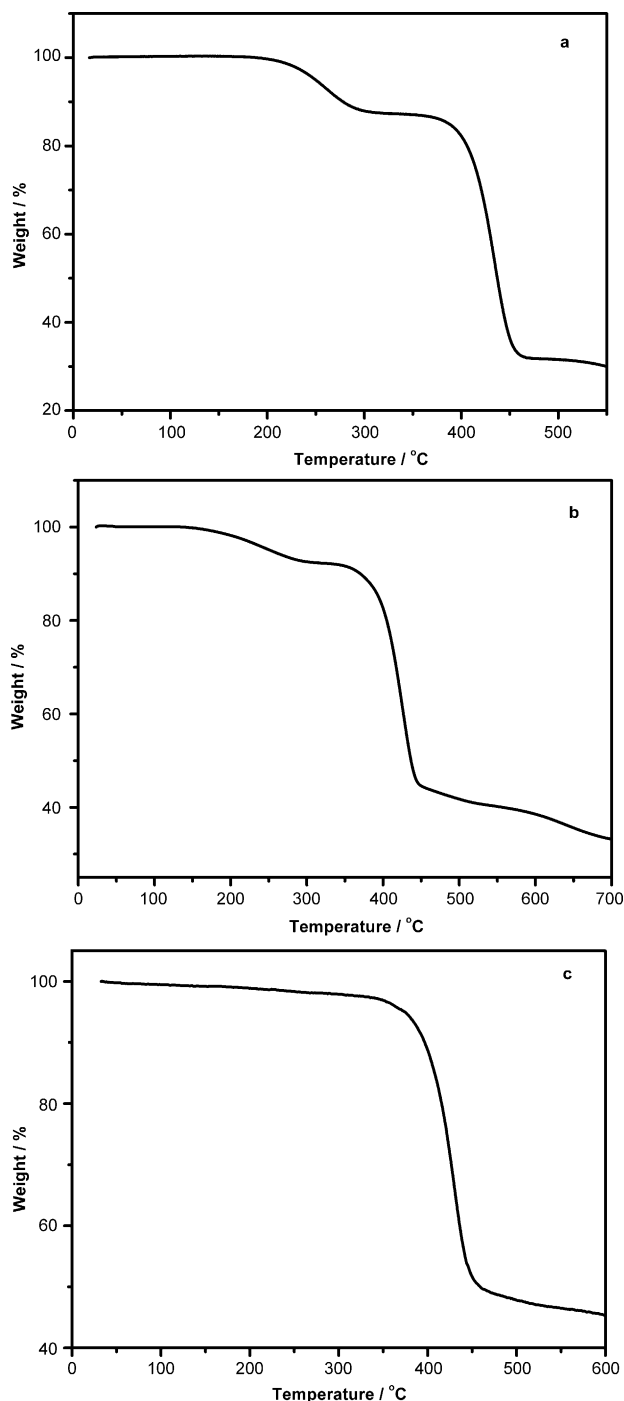


Figure 3. a) TGA thermograms of PDI, b) **PDI-Phen**, and c) **TetraPDI-PF** measured under nitrogen flow (50 mL min^{-1}) with a heating rate of $10^\circ \text{C min}^{-1}$.

tantly, the first reduction potential of **TetraPDI-PF** is about -1.20 V and obviously lower than those of PDI and **PDI-Phen**. From the first reduction value, the LUMO energies of PDI, **PDI-Phen**, and **TetraPDI-PF** are estimated to be -3.91 , -4.05 , and -3.88 eV , respectively. The relatively higher LUMO energy level of **TetraPDI-PF** is desirable for OSCs, according to the empirical formula of calculating the open-circuit voltage (V_{oc}).^[10] In addition, to investigate the electrochemical stability of **TetraPDI-PF**, the cyclic voltammetry curves are successively scanned for 15

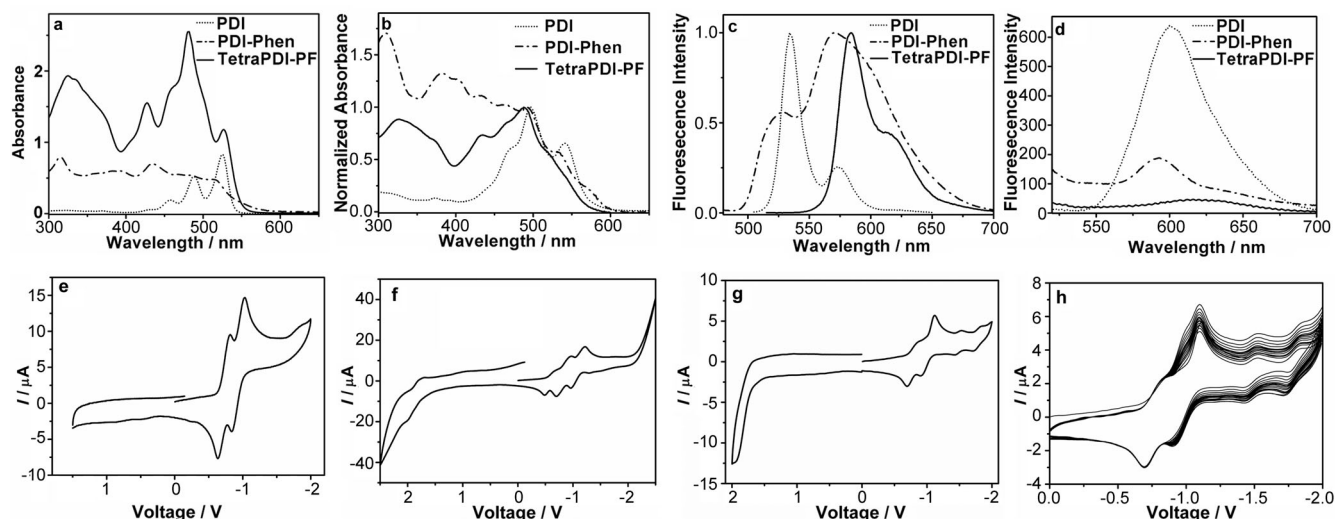


Figure 4. a) UV/Vis absorption spectra of PDI, PDI-Phen and TetraPDI-PF in dichloromethane; b) Normalized UV/Vis absorption spectra of PDI, PDI-Phen, and TetraPDI-PF in thin films; c) Normalized fluorescence spectra of PDI, PDI-Phen, and TetraPDI-PF in dichloromethane; d) Fluorescence spectra of PDI, PDI-Phen, and TetraPDI-PF in thin films; e–g) CVs of PDI, PDI-Phen and TetraPDI-PF, respectively; h) electrochemical stability of TetraPDI-PF.

Table 1. Photophysical and electrochemical properties of PDI, PDI-Phen, and TetraPDI-PF.								
Materials	$\lambda_{\text{abs}}^{[a]}$ [nm]	$\lambda_{\text{abs}}^{[b]}$ [nm]	$\lambda_{\text{em}}^{[a]}$ [nm]	$\lambda_{\text{em}}^{[b]}$ [nm]	$E_{\text{g}}^{\text{opt}}$ [eV]	$E_{1r}^{[c]}$ [V]	LUMO ^[d] [eV]	HOMO ^[d] [eV]
PDI	525	497	534	600	2.30	−1.17	−3.91	−6.21
PDI-Phen	435	492	570	593	2.24	−1.03	−4.05	−6.29
TetraPDI-PF	481	488	584	–	2.26	−1.20	−3.88	−6.14

[a] Measured in dichloromethane. [b] Measured in thin films. [c] Measured in 0.05 M solution of Bu₄NPF₆ in dichloromethane with a scan rate of 100 mV s^{−1}. [d] Based on the reference energy level of Fc/Fc⁺ (5.08 eV below vacuum).^[15]

cycles, which still remain invariable reduction potentials (Figure 4 h). TetraPDI-PF with four PDI branches inherits the excellent electrochemical stability of perylene diimides. These results reveal that TetraPDI-PF will be a potential N-type material in organic electronics.

The photostability of TetraPDI-PF is measured on a confocal fluorescence microscope by a comparison study of PDI, BODIPY, and fluorescein (the Supporting Information, Figure S3). Due to their stronger absorption in visible-light region similar to TetraPDI-PF, these fluorophores are chosen for comparison. I is the fluorescence intensities ($\lambda_{\text{ex}} = 488$ nm) of these compounds after certain periods of irradiation by blue light in the range of 460–490 nm. I_0 is the fluorescent intensity of compounds without irradiation. With the increase of irradiation time, the curves of I/I_0 record the attenuation trend of these compounds (Figure 5). The damped traces reveal that the photostability of TetraPDI-PF is the best and still maintain 99% fluorescence intensity after irradiation for 10 min using maximum laser intensity. The fluorescence intensity of PDI and BODIP are 98 and 95% of their initial intensity, which is close to value of TetraPDI-PF. However, fluorescein shows poor photostability and its damped trace decreases to 10% fluorescence intensity after irradiation for 9 min. These results reveal that

TetraPDI-PF, superior to other fluorophores of its kind, possesses the outstanding photostability because of its large, rigid conjugated framework.

The electron mobilities of PDI, PDI-Phen, and TetraPDI-PF are investigated using the steady-state space-charge-limited current (SCLC) model, which is widely applied to evaluate the charge-transporting ability in organic optoelectronics. Using the solution-processed way, the electron-only device structure is ITO/ZnO (10 nm)/PDI or PDI-Phen or TetraPDI-PF/BCP (10 nm)/LiF (1.5 nm)/Al (100 nm) (ITO = indium tin oxide, BCP = 2,9-dimethyl-4,7-diphenyl-1,10-phenanthroline). The SCLC in this case of mobility depending on the field can be approximated by:^[16]

$$J = \frac{9}{8} \epsilon \epsilon_0 \frac{E^2}{L} \mu_0 \exp(0.89\gamma\sqrt{E})$$

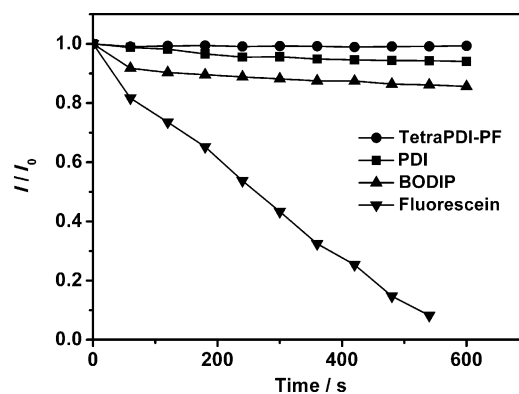


Figure 5. The changes of fluorescence intensity ($\lambda_{\text{ex}} = 488$ nm) of PDI, TetraPDI-PF, BODIPY, and fluorescein after certain periods of irradiation by the light in the range of 460–490 nm.

in which E is the electric field across the sample, ϵ and ϵ_0 are the relative dielectric constant and the permittivity of the free space, respectively, and L is the thickness of the organic layer, with μ_0 the zero-field mobility and γ describing the field activation of the mobility. As shown in Table 2, **TetraPDI-PF** has higher intrinsic electron mobility, compared with those of PDI and **PDI-Phen** under the same condition. An electron mobility of 3.52×10^{-8} , 3.57×10^{-7} , and $2.22 \times 10^{-5} \text{ cm}^2 \text{ V}^{-1} \text{ s}^{-1}$ are obtained for the film of PDI or **PDI-Phen** or **TetraPDI-PF** after annealing at 120°C for 30 min, respectively. Obviously, the electron mobility of **TetraPDI-PF** is 3 orders of magnitude higher than that of PDI. The reason is that the distortion of large rigid conjugated framework suppresses strong aggregation trend and excellent solubility is conducive to better film-forming property.

Materials	μ [$\text{cm}^2 \text{ V}^{-1} \text{ s}^{-1}$]	μ_0 [$\text{cm}^2 \text{ V}^{-1} \text{ s}^{-1}$]	γ [cm V^{-1}]
PDI	3.52×10^{-8}	9.51×10^{-10}	0.0066
PDI-Phen	3.57×10^{-7}	3.20×10^{-7}	0.0002
TetraPDI-PF	2.22×10^{-5}	1.99×10^{-5}	0.0002

To evaluate their potential as an electron acceptor in organic solar cell devices, we fabricated bulk heterojunction (BHJ) OSCs using P3HT as donor, and only investigate the weight ratio of 1:1 at the thermal annealing of 120°C . As illustrated in Figure 6 and Table 3, the device based on **TetraPDI-PF** exhibits the best performance, overwhelming those of **PDI-Phen** and PDI. The maximum power conversion efficiency (PCE) reaches 0.64% with a short-circuit current (J_{sc}) of 1.95 mA cm^{-2} , an open-circuit voltage (V_{oc}) of 0.67 V and a fill factor (FF) of 0.49 under AM 1.5 G simulated solar illumination (100 mW cm^{-2}). However, the efficiencies of **PDI-Phen** and PDI cells are only of 0.06 and 0.01%, respectively. The PCE of **TetraPDI-PF** (0.64%) is about 64 times that of the device based on PDI. We ascribe the higher efficiency to the distortion, which can inhibit intermolecular strong aggregation, good solubility, which can form the regular morphology, and higher electron mobility of **Tet-**

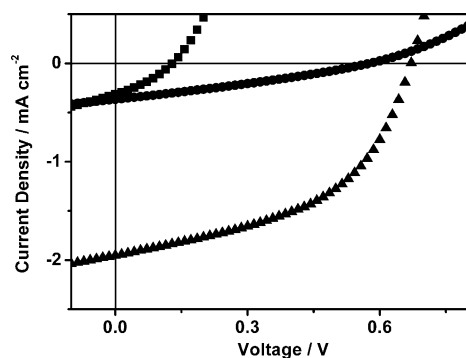


Figure 6. J/V -curves of photovoltaic devices based on P3HT:PDI (■), P3HT:PDI-Phen (●), or P3HT:TetraPDI-PF (▲).

Materials	J_{sc} [mA cm^{-2}]	V_{oc} [V]	FF	$\text{PCE}_{\text{max/av}}$ [%]
PDI	0.29	0.13	0.21	0.01/0.008
PDI-Phen	0.34	0.55	0.27	0.06/0.05
TetraPDI-PF	1.93	0.66	0.48	0.64/0.62

raPDI-PF. In addition, further studies on the BHJ OSCs are under way and will be presented in a forthcoming paper.

Atomic force microscope (AFM) height images and phase images are obtained to investigate the active layer morphologies of the OSCs. As shown in Figure 7, compared with those of PDI (6.01 nm) and **PDI-Phen** (5.84 nm), the blended film of **TetraPDI-PF**:P3HT with the high solubility and excellent film-forming property has smoother surface roughness with the root mean square (RMS) value of 4.28 nm. Corresponding to RMS, the line profile value of **TetraPDI-PF** is 30 nm, whereas the values of PDI and **PDI-Phen** are 65 and 50 nm, respectively. From their phase images, the homogeneous phase separation size of **TetraPDI-PF** can be clearly observed, and the phase separation of **TetraPDI-PF**:P3HT is appropriate, which could lead to a relative high J_{sc} , whereas the phase separation size of PDI is larger than that of **TetraPDI-PF**, which generates more geminate recombination and forms some alone islets. However, the phase separation boundary of **PDI-Phen** is not very clear. Therefore, the smoother morphology and suitable phase separation of **TetraPDI-PF**:P3HT should be beneficial to charge separation and transportation in the OSC devices.

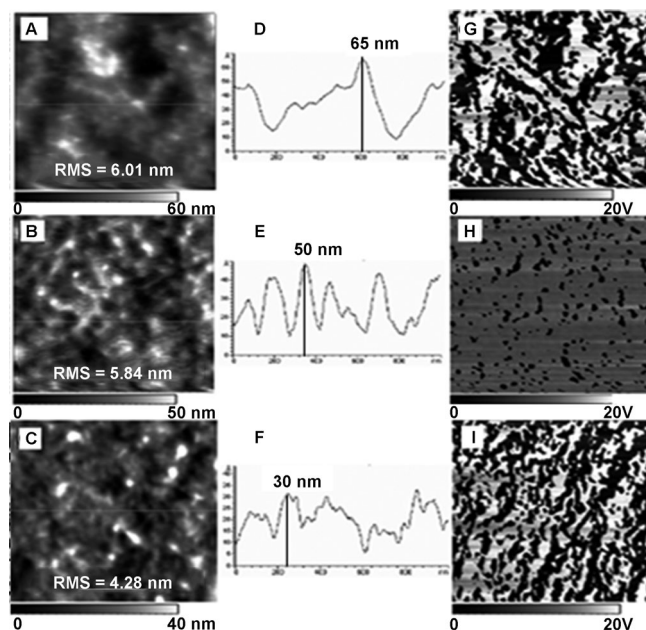


Figure 7. AFM height images ($1 \mu\text{m} \times 1 \mu\text{m}$, left), line profiles (middle) and phase images ($1 \mu\text{m} \times 1 \mu\text{m}$, right) of the blended film of P3HT:PDI (A, D, G), P3HT:PDI-Phen (B, E, H), and P3HT:TetraPDI-PF (C, F, I), respectively.

Conclusion

A new ladder-conjugated star-shaped molecule **TetraPDI-PF** containing four PDI arms and a fluorene core has been efficiently synthesized and characterized. Due to the congestion and the rigidity of the conjugated framework in which the steric hindrance results in a non-coplanar structure, **TetraPDI-PF** exhibits good solubility of as high as 155 mg mL⁻¹ in dichlorobenzene solution, compared with those of PDI (35 mg mL⁻¹) and **PDI-Phen** (70 mg mL⁻¹). Demonstrated by TGA, the oligomer shows excellent thermal stability with the T_d of 291.2 °C, which is 65 °C higher than that of PDI. Although the CV curves of **TetraPDI-PF** are successively scanned for 15 cycles, they still remain invariable reduction potentials. The oligomer also shows outstanding photostability with the order of **TetraPDI-PF** > PDI > BODIPY ≫ fluorescein after irradiation for 10 min using maximum laser intensity. And the strong broad absorption spectra range from 300 to 550 nm and high LUMO level of -3.88 eV are beneficial for promoting the light absorption and enhancing V_{oc} in the BHJ OSCs. In the electron-only devices by SCLC model, **TetraPDI-PF** exhibits higher intrinsic electron mobility of $2.22 \times 10^{-5} \text{ cm}^2 \text{ V}^{-1} \text{ s}^{-1}$, three orders of magnitude over that of PDI ($3.52 \times 10^{-8} \text{ cm}^2 \text{ V}^{-1} \text{ s}^{-1}$). The device, using **TetraPDI-PF** as non-fullerene acceptors and P3HT as donors, gives a maximum PCE of 0.64% in the BHJ OSCs.

Experimental Section

General methods

All reactants were purchased from commercial sources. Compounds 2,7-dibromophenanthraquinone, 3,6-dibromophenanthraquinone, and **7** were synthesized according to literature methods.^[17] NMR spectra were measured with a 400 MHz Bruker spectrometer using TMS as reference for ¹H and ¹³C NMR spectroscopy. Accurate mass correction is measured with MALDI TOF mass spectrometer (MALDI micro MX). Film thicknesses are determined on an Alphastep 500 surface profilometer. CV and DPV were performed in 0.05 M solution in CH₂Cl₂ with a standard commercial electrochemical analyzer in a three electrode single-component cell under argon with a scan rate of 100 mV s⁻¹. Working electrode: glassy carbon; reference electrode: Ag/AgCl; auxiliary electrode: Pt disk; internal standard: ferrocene (Fc). The energy of Fc/Fc⁺ is 5.08 eV relative to vacuum.^[15] UV/Vis absorption spectra in chloroform (CHCl₃) solution were recorded in a UV/Vis spectrophotometer (HP8453) at room temperature using a glass cuvette with a path length of 1 cm. TGA is carried out using a Mettler Toledo TGA/SDTA 851e at a heating rate of 10 °C min⁻¹ under nitrogen flow of 20 mL min⁻¹. The thin film morphology is investigated by tapping mode AFM on the Nanoscope IV system commercialized by Veeco.

Compound 3: A mixture of 2,7-dibromophenanthraquinone (2 g, 5.46 mmol), ethylene glycol (6.1 mL, 109.83 mmol), *p*-toluene sulfonic acid (132 mg, 0.765 mmol) was heated to reflux by water separator in the toluene solution under argon atmosphere. Upon cooling to RT, the white precipitate was collected by filtration and washed with H₂O, MeOH, and Et₂O yielding compound **3** (1.268 g, 51%) as a white solid. M.p. 262.6–262.9 °C; ¹H NMR (400 MHz, CDCl₃, 25 °C, TMS): δ = 7.88 (d, 1H, CH), 7.70 (d, 1H, CH), 7.58 (q, 1H, CH), 4.22 (s, 2H, CH₂), 3.66 ppm (s, 2H, CH₂); ¹³C NMR

(100 MHz, CDCl₃, 25 °C): δ = 167.97, 134.98, 133.27, 131.33, 129.63, 125.64, 123.31, 92.19, 61.60 ppm; MS (LC/Q-TOF-MS, pos. mode): *m/z* calcd for C₁₈H₁₄O₄Na: 474.9157 [*M*+Na]⁺; found: 474.9150.

Compound 4: A mixture of compound **3** (300 mg, 0.66 mmol), bis(pinacolato)diboron (504 mg, 1.98 mmol), potassium acetate (389 mg, 3.96 mmol), [1,1'-bis(diphenylphosphino)ferrocene]palladium(II) chloride (24 mg) was stirred at 90 °C for 24 h in the toluene solution under argon atmosphere. Then, the crude product is purified through silica gel column chromatography with CH₂Cl₂ and MeOH (v/v; 50:1) as eluent. Compound **4** was obtained as white solid (200 mg, 55%). M.p. > 300 °C; ¹H NMR (400 MHz, CDCl₃, 25 °C, TMS): δ = 8.20 (s, 1H, CH), 7.92 (q, 2H, CH), 4.23 (s, 2H, CH₂), 3.68 (s, 2H, CH₂), 1.34 ppm (s, 12H, CH₃); ¹³C NMR (100 MHz, CDCl₃, 25 °C): δ = 136.29, 135.60, 132.68, 132.56, 132.32, 130.20, 129.61, 124.38, 123.52, 123.18, 92.88, 84.02, 83.64, 61.59, 53.58, 29.85, 25.05, 19.32 ppm; MS (MALDI-TOF-MS, pos. mode): *m/z* calcd for C₃₀H₃₈O₈B₂Na: 571.2650 [*M*+Na]⁺; found: 571.2617.

Compound 5: A mixture of 1-bromoperylene diimide (728 mg, 0.635 mmol), compound **4** (179 mg, 0.327 mmol), K₂CO₃ (226 mg, 1.635 mmol), H₂O (1.6 mL), and [Pd(PPh₃)₄] (42 mg) was heated to 70 °C for 16 h in THF under argon atmosphere. Then, the crude product was purified through silica gel column chromatography with CH₂Cl₂ and *n*-hexane (v/v; 2:1) as eluent. Compound **5** is obtained as red solid (624 mg, 81%). M.p. 268.8–270 °C; ¹H NMR (400 MHz, CDCl₃, 25 °C, TMS): δ = 8.73–8.57 (m, 3H), 8.36 (dd, 2H), 8.10 (dd, 4H), 7.69 (d, 1H), 5.37 (d, 2H), 4.00 (s, 2H), 3.56 (s, 2H), 2.43 (d, 4H), 2.08–1.89 (m, 4H), 1.54–1.12 (m, 84H), 0.82 ppm (dd, 15H); ¹³C NMR (100 MHz, CDCl₃, 25 °C): δ = 164.96, 164.78, 163.86, 163.67, 147.91, 147.77, 147.54, 147.24, 146.98, 146.18, 145.31, 143.57, 141.52, 140.85, 138.70, 135.73, 135.02, 134.54, 132.82, 131.04, 130.39, 129.40, 128.83, 128.31, 127.75, 127.06, 126.36, 124.14, 123.79, 123.28, 122.97, 122.49, 92.66, 61.61, 54.89, 35.05, 34.70, 32.56, 32.07, 31.61, 30.48, 30.36, 29.77, 29.50, 27.13, 22.84, 14.26 ppm; MS (MALDI-TOF-MS, pos. mode): *m/z* calcd for C₁₅₈H₂₁₆N₄O₁₂Na: 2384.6313 [*M*+Na]⁺; found: 2384.6470.

Compound 8: A mixture of compound **7** (3 g, 6.61 mmol), bis(pinacolato)diboron (4.36 g, 17.18 mmol), potassium acetate (3.89 g, 39.64 mmol), [1,1'-bis(diphenylphosphino)ferrocene]palladium(II) chloride (248 mg) was stirred at 90 °C for 24 h in the toluene solution under argon atmosphere. Then, the crude product is purified through silica gel column chromatography with CH₂Cl₂ and MeOH (v/v; 50:1) as eluent. Compound **8** was obtained as pale-yellow solid (3.35 g, 93%). M.p. > 300 °C; ¹H NMR (400 MHz, CDCl₃, 25 °C, TMS): δ = 8.33 (d, 1H, CH), 7.79 (t, 1H, CH), 7.67 (d, 1H, CH), 4.12 (s, 2H, CH₂), 3.57 (s, 2H, CH₂), 1.32 ppm (s, 12H, CH₃); ¹³C NMR (100 MHz, CDCl₃, 25 °C): δ = 135.60, 135.37, 132.66, 130.64, 125.43, 92.75, 84.20, 66.52, 61.64, 25.04 ppm; MS (MALDI-TOF-MS, pos. mode): *m/z* calcd for C₃₀H₃₈B₂O₈: 548.2753 [*M*]⁺; found: 548.2726.

Compound 9: A mixture of 1-bromoperylene diimide (1.4 g, 1.26 mmol), compound **8** (344 mg, 0.628 mmol), K₂CO₃ (434 mg, 3.14 mmol), H₂O (1.6 mL), and [Pd(PPh₃)₄] (98 mg) was heated to 90 °C for 13 h in toluene under argon atmosphere. Then, the crude product was purified through silica gel column chromatography with CH₂Cl₂ and *n*-hexane (v/v; 2:1) as eluent. Compound **9** was obtained as red solid (933 mg, 63%). M.p. > 300 °C; ¹H NMR (400 MHz, CDCl₃, 25 °C, TMS): δ = 8.84 (m, 1H), 8.64–8.51 (m, 1H), 8.47–8.15 (m, 2H), 7.88 (t, 1H), 5.54 (t, 1H), 4.19 (t, 1H), 3.73 (d, 1H), 2.79–2.48 (m, 2H), 2.33–2.04 (m, 3H), 1.82–1.28 (m, 50H), 1.03 ppm (dd, 8H); ¹³C NMR (100 MHz, CDCl₃, 25 °C): δ = 164.79, 163.72, 144.74, 140.70, 135.06, 134.50, 130.46, 129.59, 129.38, 128.80, 128.18, 127.65, 123.67, 122.91, 92.57, 54.86, 53.56, 32.48, 32.02, 29.73, 29.45, 27.09, 27.01, 22.79, 19.31, 19.11, 17.06,

14.23 ppm; MS (MALDI-TOF-MS, pos. mode): m/z calcd for $C_{158}H_{216}N_4O_{12}Na$: 2384.6313 $[M+Na]^+$; found: 2384.6375.

Compound dg-PDI-Phen: The compound **dg-PDI-Phen** can be prepared by two synthetic methods. *Method 1:* A mixture of compound **5** (1.1 g, 0.465 mmol) and a catalytic amount of iodine was heated to 110 °C for 6 h in toluene under a sunlight atmosphere. The mixture was evaporated and the crude product was purified by silica gel column chromatography with dichloromethane and *n*-hexane (v/v; 2:1) as eluent. Compound **dg-PDI-Phen** was obtained as a red solid (235 mg, 21%). *Method 2:* A mixture of compound **9** (933 mg, 0.395 mmol) and a catalytic amount of iodine was heated to 110 °C for 6 h in toluene under sunlight atmosphere. The mixture was evaporated and the crude product was purified by silica gel column chromatography with dichloromethane and *n*-hexane as eluent. Compound **dg-PDI-Phen** was obtained as red solid (655 mg, 70%). M.p. > 300 °C. 1H NMR (400 MHz, $CDCl_3$, 25 °C, TMS): δ = 10.42 (s, 1H), 9.72 (s, 1H), 9.31–8.78 (m, 6H), 5.81 (s, 1H), 5.38 (s, 1H), 4.28 (s, 1H), 3.57 (s, 1H), 2.98 (s, 2H), 2.43 (d, 7H), 1.99–0.66 ppm (m, 104H); ^{13}C NMR (100 MHz, $CDCl_3$, 25 °C): δ = 164.94, 163.84, 143.57, 140.84, 135.72, 135.02, 134.54, 132.82, 131.71, 131.05, 130.48, 129.40, 128.82, 128.31, 127.75, 127.11, 126.32, 123.79, 123.22, 122.97, 122.47, 92.66, 61.63, 55.01, 54.81, 32.56, 32.07, 29.77, 29.50, 27.14, 22.84, 14.28 ppm; MS (MALDI-TOF-MS, pos. mode): m/z calcd for $C_{158}H_{212}N_4O_{12}Na$: 2380.5999 $[M+Na]^+$; found: 2380.6194.

Compound PDI-Phen: A mixture of compound **dg-PDI-Phen** (735 mg, 0.312 mmol), *p*-toluene sulfonic acid (5 g, 26.3 mmol) was heated to 125 °C for 10 h. Then, the crude product was purified through silica gel column chromatography with CH_2Cl_2 and *n*-hexane (v/v; 1:1) as eluent. Compound **PDI-Phen** was obtained as red solid (632 mg, 90%). M.p.: 295.7–296.3 °C. 1H NMR (400 MHz, $CDCl_3$, 25 °C, TMS): δ = 10.05–9.32 (m, 4H), 9.08 (d, J = 66.8 Hz, 3H), 8.68 (s, 2H), 6.00 (s, 1H), 5.76 (s, 1H), 3.32–0.80 ppm (m, 129H); ^{13}C NMR (100 MHz, $CDCl_3$, 25 °C): δ = 178.80, 164.97, 164.25, 163.42, 162.57, 133.73, 132.63, 131.67, 130.89, 130.15, 128.59, 127.43, 126.85, 123.51, 123.00, 120.03, 55.56, 33.26, 32.09, 31.60, 29.86, 27.83, 22.83, 14.24 ppm; MS (MALDI-TOF-MS, pos. mode): m/z calcd for $C_{154}H_{204}N_4O_{10}Na$: 2292.5475 $[M+Na]^+$; found: 2292.5659.

Compound TetraPDI-PF: A mixture of compound **PDI-Phen** (100 mg, 0.044 mmol) and 2,3,6,7-tetraamino-9,9-bis(2-ethylhexyl)-fluorene was heated to 120 °C for 6 h in $CHCl_3$ and glacial acetic acid solution under argon atmosphere. The mixture is evaporated and the crude product was purified by silica gel column chromatography with dichloromethane and *n*-hexane (v/v; 3:1) as eluent. Compound **TetraPDI-PF** was obtained as red solid (235 mg, 74%). M.p. > 300 °C. 1H NMR (400 MHz, $CDCl_3$, 25 °C, TMS): δ = 11.51 (d, 1H), 11.34–10.80 (m, 3H), 9.69–8.80 (m, 5H), 5.34 (d, 2H), 3.01–1.87 (m, 9H), 1.76–0.42 ppm (m, 98H); ^{13}C NMR (100 MHz, $CDCl_3$, 25 °C): δ = 165.75, 165.48, 165.33, 165.04, 164.66, 164.35, 164.27–164.18, 155.43, 143.91, 143.20, 143.04–142.99, 142.96–142.93, 134.36, 131.60, 131.47, 130.88, 130.60, 130.11, 129.83, 129.50, 128.88, 128.14, 126.37–126.20, 126.09, 125.33, 125.00, 124.11, 123.61, 123.38–123.18, 122.84, 121.78, 119.76, 55.95, 55.86–55.69, 55.55, 48.11–47.83, 35.60, 33.48, 33.25, 33.00, 32.41, 32.22, 32.05, 31.80, 30.34, 30.12, 29.89, 29.81, 29.66, 29.51, 29.32, 28.28, 27.92, 27.68, 27.37, 27.10, 22.79, 22.61, 14.21, 14.08, 13.95–13.89, 13.87–13.83, 10.62 ppm; MS (MALDI-TOF-MS, neg. mode): m/z calcd for $C_{336}H_{444}N_{12}O_{16}$: 4907.1914 $[M]^-$; found: 4907.8926.

Photostability measurements

The photostability of these compounds was evaluated by Nikon C1 confocal microscope. The structures of BODIPY and fluorescein are

shown in Scheme S2 (the Supporting Information). First, the solution of sample is sealed in a microscope concave slide with cover slip (the concentration of all the compounds is 10^{-5} M; PDI, **TetraPDI-PF**, and BODIPY were dissolved in toluene; fluorescein was dissolved in an aqueous solution with pH 11; all solutions are air saturated). Then it is placed on the objective lens of the confocal microscope, and irradiated by the light in the range of 460–490 nm using a band pass filter that transmits from 460 to 490 nm with the same light intensity. The fluorescent images are recorded with Nikon C1 confocal fluorescence microscope exciting at 488 nm (Ar Laser) at different lengths of time after exposure. The average fluorescent intensity is calculated from the software EZ-C1 3.90 Free-viewer.

Device preparation and characterization

BHJ organic device preparation proceeds as follows. A $15 \Omega \text{ cm}^{-2}$ resistor of indium-doped tin oxide (ITO) substrate is purchased from Xiangcheng Science and Technology Co., Ltd., and then the substrates undergo a cleaned course in an ultrasonic bath with acetone, ethanol, and ultrapure water and dried for 1 h under a blast dry oven. Subsequently, the glasses were cleaned in oxygen plasma treatment for 10 min, and a PEDOT:PSS (Clevios P VP Al 4083, H.C. Starck) solution is then spin-coated at 2000 rpm for 60 s onto the cleaned ITO surface, resulting in a thickness of ≈ 40 nm, as determined with a Dektak surface profilometer. The PEDOT:PSS layer is annealed for 30 min at 120 °C in air. A solution of active layer P3HT (Rieke No. 4002-E) and PDI, **PDI-Phen** or **TetraPDI-PF** were simultaneously dissolved in dichlorobenzene in a weight ratio of 1:1 at a concentration of 16 mg mL^{-1} and stirred for 1 h at a temperature of 90 °C in an oil bath. Before deposition of the active layer, the mixed solution of P3HT:PDI, **PDI-Phen** or **TetraPDI-PF** is filtered through a polytetrafluoroethylene (PTFE) syringe filter (0.45 μm pore size). The active layer is then spin-coated on top of the PEDOT:PSS film at 1200 rpm (dichlorobenzene) for 18 s resulting in a film thickness of ≈ 100 nm. The films are annealed at 120 °C for 30 min in the vacuum state. The 10 nm thick 2,9-dimethyl-4,7-diphenyl-1,10-phenanthroline (BCP) and 1.5 nm thick LiF layer is thermally deposited under a pressure of 2×10^{-4} Pa, followed by aluminum counter electrodes are evaporated through a shadow mask on top of the active layer with a thickness of ≈ 100 nm. The active area of the pixels, as defined by the overlap of anode and cathode area, is 0.20 cm^2 . The photovoltaic performance was determined under simulated sunlight, using a commercial solar simulator (Zolix ss150 solar simulator, China).

Acknowledgements

This work is supported by National Natural Science Foundation of China (No. 21174022), National Basic Research Program of China (No. 2013CB733702), Fundamental Research Funds for the Central Universities (No. 1004852012) and Specialized Research Fund for the Doctoral Program of Higher Education (No. 20110041110009).

Keywords: cyclic voltammetry · dyes/pigments · electron-deficient compounds · electron transport · oligomers

- [1] a) V. Kamm, G. Battagliarin, I. A. Howard, W. Pisula, A. Mavrinskiy, C. Li, Müllen, K. F. Laquai, *Adv. Energy Mater.* **2011**, *1*, 297–302; b) T. Zhou, T. Jia, B. Kang, F. Li, M. Fahlman, Y. Wang, *Adv. Energy Mater.* **2011**, *1*, 431–439.

- [2] a) J. You, C. C. Chen, L. Dou, S. Murase, H. S. Duan, S. A. Hawks, T. Xu, H. J. Son, L. Yu, G. Li, *Adv. Mater.* **2012**, *24*, 5267–5272; b) J. You, L. Dou, K. Yoshimura, T. Kato, K. Ohya, T. Moriarty, K. Emery, C.-C. Chen, J. Gao, G. Li, Y. Yang, *Nat. Commun.* **2013**, *4*, 1446–1455; c) G. Li, R. Zhu, Y. Yang, *Nat. Photonics* **2012**, *6*, 153–161; d) Z. He, C. Zhong, S. Su, M. Xu, H. Wu, Y. Cao, *Nat. Photonics* **2012**, *6*, 593–597; e) J. You, C. C. Chen, Z. Hong, K. Yoshimura, K. Ohya, R. Xu, S. Ye, J. Gao, G. Li, Y. Yang, *Adv. Mater.* **2013**, *25*, 3973–3978.
- [3] a) T. V. Pho, F. M. Toma, M. L. Chabiny, F. Wudl, *Angew. Chem.* **2013**, *125*, 1486–1491; *Angew. Chem. Int. Ed.* **2013**, *52*, 1446–1451; b) E. Zhou, J. Cong, Q. Wei, K. Tajima, C. Yang, K. Hashimoto, *Angew. Chem.* **2011**, *123*, 2851–2855; *Angew. Chem. Int. Ed.* **2011**, *50*, 2799–2803; c) J. T. Bloking, X. Han, A. T. Higgs, J. P. Kastrop, L. Pandey, J. E. Norton, C. Risko, C. E. Chen, J.-L. Brédas, M. D. McGehee, *Chem. Mater.* **2011**, *23*, 5484–5490; d) G. Sharma, P. Suresh, J. A. Mikroyannidis, M. M. Stylianakis, *J. Mater. Chem.* **2010**, *20*, 561–567; e) S. Rajaram, R. Shivanna, S. K. Kandappa, K. J. Narayan, *J. Phys. Chem. Lett.* **2012**, *3*, 2405–2408.
- [4] a) Q. Xu, J. Wang, S. Chen, W. Li, H. Wang, *Express Polym. Lett.* **2013**, *7*, 842–851; b) H. Qian, F. Negri, C. Wang, Z. Wang, *J. Am. Chem. Soc.* **2008**, *130*, 17970–17976; c) W. Yue, A. Lv, J. Gao, W. Jiang, L. Hao, C. Li, Y. Li, L. E. Polander, S. Barlow, W. Hu, *J. Am. Chem. Soc.* **2012**, *134*, 5770–5773; d) W. Zhou, Y. Wen, L. Ma, Y. Liu, X. Zhan, *Macromolecules* **2012**, *45*, 4115–4121; e) M. M. Durban, P. D. Kazarinoff, Y. Segawa, C. K. Luscombe, *Macromolecules* **2011**, *44*, 4721–4728; f) X. Zhan, Z. A. Tan, B. Domercq, Z. An, X. Zhang, S. Barlow, Y. Li, D. Zhu, B. Kippelen, S. R. Marder, *J. Am. Chem. Soc.* **2007**, *129*, 7246–7247; g) X. Zhan, Z. A. Tan, E. Zhou, Y. Li, R. Misra, A. Grant, B. Domercq, X.-H. Zhang, Z. An, X. Zhang, *J. Mater. Chem.* **2009**, *19*, 5794–5803; h) Z. Chen, Y. Zheng, H. Yan, A. Facchetti, *J. Am. Chem. Soc.* **2008**, *130*, 8–9; i) H. Li, F. S. Kim, G. Ren, S. A. Jenekhe, *J. Am. Chem. Soc.* **2013**, *135*, 14920–14923; j) T. Earmme, Y.-J. Hwang, N. M. Murari, S. Subramaniam, S. A. Jenekhe, *J. Am. Chem. Soc.* **2013**, *135*, 14960–14963.
- [5] A. Babel, S. A. Jenekhe, *J. Am. Chem. Soc.* **2003**, *125*, 13656–13657.
- [6] H. Li, F. S. Kim, G. Ren, E. C. Hollenbeck, S. Subramaniam, S. A. Jenekhe, *Angew. Chem.* **2013**, *125*, 5623–5627; *Angew. Chem. Int. Ed.* **2013**, *52*, 5513–5517.
- [7] Z. Yuan, S.-L. Lee, L. Chen, C. Li, K. S. Mali, S. De Feyter, K. Müllen, *Chem. Eur. J.* **2013**, *19*, 11842–11846.
- [8] a) J. Cremer, P. Bäuerle, *J. Mater. Chem.* **2006**, *16*, 874–884; b) M. Sonntag, K. Kreger, D. Hanft, P. Strohriegel, S. Setayesh, D. de Leeuw, *Chem. Mater.* **2005**, *17*, 3031–3039; c) Y. Sun, K. Xiao, Y. Liu, J. Wang, J. Pei, G. Yu, D. Zhu, *Adv. Funct. Mater.* **2005**, *15*, 818–822; d) H. Shang, H. Fan, Y. Liu, W. Hu, Y. Li, X. Zhan, *Adv. Mater.* **2011**, *23*, 1554–1557.
- [9] a) G. C. Bazan, W. J. Oldham, R. J. Lachicotte, S. Tretiak, V. Chernyak, S. Mukamel, *J. Am. Chem. Soc.* **1998**, *120*, 9188–9204; b) M. R. Robinson, S. Wang, G. Bazan, Y. Cao, *Adv. Mater.* **2000**, *12*, 1701–1704; c) S. Laschat, A. Baro, N. Steinke, F. Giesselmann, C. Hägele, G. Scalia, R. Judele, E. Kapatsina, S. Sauer, A. Schreivogel, *Angew. Chem.* **2007**, *119*, 4916–4973; *Angew. Chem. Int. Ed.* **2007**, *46*, 4832–4887; d) J. Wu, W. Pisula, K. Müllen, *Chem. Rev.* **2007**, *107*, 718–747; e) T. Kato, T. Yasuda, Y. Kamikawa, M. Yoshio, *Chem. Commun.* **2009**, 729–739.
- [10] Y. Lin, P. Cheng, Y. Li, X. Zhan, *Chem. Commun.* **2012**, *48*, 4773–4775.
- [11] Z. Yuan, Y. Xiao, Y. Yang, T. Xiong, *Macromolecules* **2011**, *44*, 1788–1791.
- [12] Y. Xie, X. Zhang, Y. Xiao, Y. Zhang, F. Zhou, J. Qi, J. Qu, *Chem. Commun.* **2012**, *48*, 4338–4340.
- [13] Z. Zhao, Y. Xiao, Y. Zhang, H. Wang, *RSC Adv.* **2013**, *3*, 21373–21376.
- [14] X. Li, Y. Xiao, X. Qian, *Org. Lett.* **2008**, *10*, 2885–2888.
- [15] B. C. Thompson, Y.-G. Kim, T. D. McCarley, J. R. Reynolds, *J. Am. Chem. Soc.* **2006**, *128*, 12714–12725.
- [16] P. N. Murgatroyd, *J. Phys. D* **1970**, *3*, 151–156.
- [17] a) J. E. Gautrot, P. Hodge, M. Helliwell, J. Raftery, D. Cupertino, *J. Mater. Chem.* **2009**, *19*, 4148–4156; b) L. A. Estrada, D. C. Neckers, *Org. Lett.* **2011**, *13*, 3304–3307.

Received: February 10, 2014

Published online on ■■■■, 2014

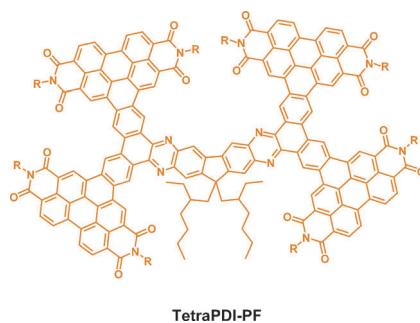
FULL PAPER

■ Electron-Deficient Compounds

Y. Zhang, L. Chen,* K. Zhang, H. Wang,
Y. Xiao*



A Soluble Ladder-Conjugated Star-Shaped Oligomer Composed of Four Perylene Diimide Branches and a Fluorene Core: Synthesis and Properties



Ladder to the stars: A new electron-transporting material containing four perylene diimide branches, which exhibits high solubility and excellent thermal stability, electrochemical stability, and photostability, was efficiently synthesized. The intrinsic electron mobility and the photovoltaic performance with **TetraPDI-PF** as non-fullerene acceptors and P3HT as electron donors were also investigated (see figure).